EFFECT OF Y, Au AND YAu NANOSANDWICHING ON THE STRUCTURAL, OPTICAL AND DIELECTRIC PROPERTIES OF ZnSe THIN FILMS

A. F. QASRAWI[a,b,*], M. F. TALEB[a]
a Department of Physics, Arab American University, Jenin, Palestine
bGroup of physics, Faculty of Engineering, Atilim University, 06836 Ankara, Turkey

In this article, we report the effects of insertion of yttrium, gold and yttrium-gold (YAu) metallic nano-slabs on the structural, optical and dielectric properties of ZnSe thin films. The ZnSe thin films which are prepared by the thermal evaporation technique under vacuum pressure of 10^{-5} mbar exhibit hexagonal structure. While the insertion of the 70 nm thick Y layers does not alter the lattice parameters and stress values, the Au and YAu layers increased the lattice parameters along the *a-* and *c*-axes and decreased the stress values. In addition, the insertion of these metallic layers slightly alters the value of the energy band gap and increases the width of the interbands. The light absorbability are increased by 1.4, 2.0 and 2.4 times upon insertion of Y, Au and YAu, slabs, respectively. On the other hand, the dielectric and optical conductivity analyses has shown that the use of the YAu stacked metal layers increases the real part of the dielectric constant, the optical conductivity, the drift mobility and extended the plasmon frequency range from 35.1 to 254.0 $(\Omega cm)^{-1}$, from 1098 to 1766 cm^2/Vs and from 0.94-3.11 GHz to 2.13-4.83 GHz, respectively. The insertion of the two stacked metallic layers between two layers of ZnSe makes the ZnSe more appropriated for thin film transistor technology.

1. Introduction

ZnSe thin films are of interest due to their wide range of technological applications. They have been employed for infrared imaging [1], visible and ultraviolet ray detection [2,3]. Recently, remarkable improvements in the properties of ZnSe films that nominate them for use in thermal imaging systems are reported [1]. In another study, ZnSe/ZnTe superlattices are used as base to fabricate photodetectors that exhibit high current sensitivity and high external quantum efficiency [2]. A maximum current sensitivity of 220 mA/W is recorded at 620 nm and at 870 nm. The external quantum efficiency for this photodetector reached 44% [2]. In addition, ZnSe/ZnS core/shell quantum dots as photodetectors show tunable photo responsivity for the UV light. This device is found to be functional even after 1000 bending cycles [3].

Attempts to enhance the performance of ZnSe employed both of the doping [4, 5] and nanosandwiching techniques [6, 7]. As for example, the doping of ZnSe with Fe make them attractive for use as mid-infrared laser active media [4]. A laser emission of linewidth of 4.24 μm is achieved when the crystals are pumped with Er:YAG laser at room temperature. In addition, Mn doped ZnSe is reported to exhibit unique fluorescent and magnetic properties that advances ZnSe as attractive material for use in fluorescence/magnetic resonance dual mode imaging [5]. On the other hand, the Ag nanosandwiching between two layers of ZnSe [6] thin films make the material suitable for use as transparent electrodes in optoelectronic devices. The Ag nanosandwiching increased the mobility of the free electrons in ZnSe to 17.22 cm²/Vs. Optically, the indium nanosandwiching between two layers of ZnSe is observed to enhance the light absorbability near 2.38 eV and to shrink the energy band gap of ZnSe.

---

[*]Corresponding author: atef.qasrawi@atilim.edu.tr

The nanosandwiching of ZnSe with Ag and with indium motivated us to study the effect of yttrium and gold nanosandwiching effects on the structural, optical, dielectric and optical conduction parameters of ZnSe films. Although the nanosandwiching of Ag and In provide good alternative to the doping technique and literature data reported remarkable enhancements in the optical performance of ZnSe via the nanosandwiching procedure, yet, literature data report no works about the nanosandwiching effects on the dielectric and optical conductivity parameters of this material. Thus, here in this article, we will report the effect of two different stacked nano-films on improving the dielectric and optical conductivity performance of ZnSe thin films.

2. Experimental details

Zinc selenide films of thicknesses of 500 nm are grown onto ultrasonically cleaned glass substrates from high purity ZnSe powders (Alpha Aeser 99.99%) in a thermal vacuum system under a pressure of 10^{-5} mbar. Some of the fabricated ZnSe films are used as substrate to grow thin layers of high purity (99.999%) yttrium (70 nm), Au (70 nm) and YAu (140 nm) films. The thicknesses of the metal film are selected to be 70 nm to assure the formation of a complete thin layer. The produced ZnSe/(Y, Au, YAu) films are, then, used as substrate to grow another film of ZnSe so that the ZnSe//Y/ZnSe, ZnSe/Au/ZnSe and ZnSe/YAu/ZnSe nanosandwiched structures are created. The thicknesses are controlled by an in situ STM-2 thickness monitor connected to the quartz crystal inside the vacuum chamber. Cu Kα radiation Miniflex 600 X-ray unit is used to explore the structural modifications that are associated with the nanosandwiching process. The optical measurements are carried out with the help of Evolution 300 spectrophotometer

3. Results and discussion

The X-ray diffraction (XRD) patterns which are recorded for ZnSe, ZnSe/Y/ZnSe, ZnSe/Au/ZnSe and ZnSe/YAu/ZnSe nanosandwiched films are presented in Fig. 1. The analysis of the intensive peaks which are subjected to "TREOR 92" software package analysis reveals a hexagonal structure for two stacked layers of ZnSe and for ZnSe/Y/ZnSe, ZnSe/Au/ZnSe and ZnSe/YAu/ZnSe thin films. As it is displayed in the Fig. 1, for ZnSe film, a peak of maximum height is observed at $2\theta = 28.1°$ and a peak of minor height occurs at $2\theta = 25.4°$. These two peaks are, respectively, assigned to the scattering from the (002) and (100) hexagonal phase of ZnSe planes in accordance with the published data [8]. The lattice parameters (a and c) for the studied films are calculated with the help of the formula, $d_{hkl}^{-2} = \frac{4}{3}(\frac{h^2+k^2+hk}{a^2})+\frac{l^2}{c^2}$ with (hkl) being the Miller indices and d is interplanar spacing. The lattice parameters values with the diffraction angle (2θ) value and peak intensities (I) are presented in Table 1. The lattice parameters value being a = 4.051 Å and c = 6.354 Å for ZnSe, are consistent with literature data [9, 10].
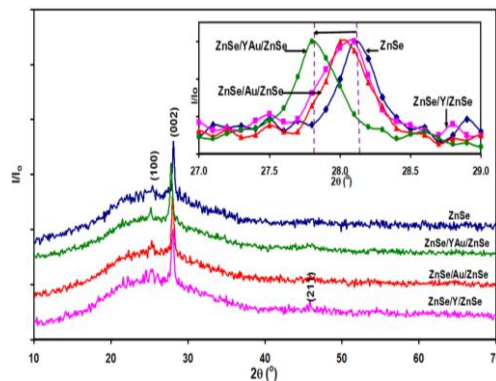

Fig. 1. The x-ray diffraction patterns for ZnSe, ZnSe/Y/ZnSe, ZnSe/Au/ZnSe and ZnSe/YAu/ZnSe films.

The XRD patterns for ZnSe/Y/ZnSe sandwiched films as illustrated in Fig. 1 exhibited similar peak positions at $2\theta = 28.1°$ and $2\theta = 25.4°$ which also relate to hexagonal ZnSe with (002) and (100) planes. Compared to that of ZnSe (inset of Fig. 1), the peak width increases indicating a deformation in the structure. In addition, a new peak appeared for ZnSe/Y/ZnSe at $2\theta = 45.8°$. This peak relates to hexagonal ZnSe being oriented in the (211) direction [8] and it disappeared in the other films. The calculated lattice parameters values are found to be a = 4.051 Å and c = 6.354 Å for ZnSe/Y/ZnSe. The appearance of the (211) reflection plane in the XRD of the ZnSe/Y/ZnSe indicates a metal induced crystallization process in ZnSe associated with the presence of yttrium [11]. In addition, the resulting XRD pattern for ZnSe/Au/ZnSe is also displayed in Fig. 1. Likewise, the peak width increased when compared to that of ZnSe. The peaks position shifts to $2\theta = 28.0°$ and $2\theta = 25.3°$. The calculated lattice parameters values are a = 4.066 Å and c = 6.376 Å for ZnSe/Au/ZnSe. On the other hand, the X-ray diffraction patterns for ZnSe/YAu/ZnSe which is illustrated in Fig. 1 show a clear shift (enlarged in inset of Fig. 1) in the peaks position to $2\theta = 27.8°$ and $2\theta = 25.2°$. Narrower peak for YAu sandwiched films leads to more ideal structure. Namely, as shown in Table1, the presence of YAu stacked layers between two layers of ZnSe resulted in more intensive XRD patterns, the calculated lattice parameters values are a = 4.082 Å and c = 6.421 Å.

In order to understand the structural characteristics of ZnSe, ZnSe/Y/ZnSe, ZnSe/Au/ZnSe and ZnSe/YAu/ZnSe sandwiched films. The grain size (D), stacking fault (SF), stress (S), dislocation density (δ) and micro-strain (ε), are calculated with the previously published equations [7]. The values are illustrated in Table 1. It is clear from the table that the presence of Y, Au and YAu highly increased the intensity indicating better crystallization process in ZnSe as we mention before. The nanosandwiching of yttrium layers between two ZnSe layers has no effect on the lattice parameters and the stress (*S*) along the *a* and *c*- axes. But yttrium reduces the grain size (*D*), the stacking fault (*SF*), dislocation density (δ) and increased the micro-strain (ε) (Table 1). Since the ionic radius of Y^{+3} is 102 pm [12] and that of Zn^{+2} is 74 pm [13], it is impossible for Y^{+3} to replace the vacant sites of Zn^{+2} and form $Y − Se$ bond. The Y metal is one of the F_{m-3c} space group and exhibit an FCC structure of lattice constant 4.930 Å [14], which indicate a lattice mismatch of ~21% and ~22% along the *a*- and *c*- axes, respectively. Large mismatched films are reported to causes a high defect density in the films. Large defect density can enable materials to be used for producing a highly efficient light emitting diodes (LED) [15].

For the ZnSe/Au/ZnSe structure, the lattice parameter increased. As illustrated in Table 1, while the grain size (*D*) and the stress (*S*) is reduced, the stacking faults (*SF*), dislocation density (δ) and micro-strain (ε) increased. From the chemical point of view, the ionic radius of Au^+ being 137 pm [16] is larger than that of Zn^{+2} (74 pm) [13]. In this case, substituting Au^+ in Zn^{+2} sites is not possible. Thus Au^+ ions can occupy interstitial positions between Zn-Se bonds. The Au metal belongs to F_{m-3m} space group and exhibit an *FCC* structure of lattice constant values of 4.078 Å [17], which indicate a large lattice mismatch of ~ 35% along the *c*-axes. On the other hand, it indicates a good lattice match of 0.66% along the *a*-axis. This lattice match along *a*-axes has good influence on the electrical and thermal conductivity performances [15].

The nanosandwiching of the YAu alloy layer between two ZnSe layers is more effective in enhancing the ZnSe crystallinity. The idea of stacking two different metals is to have different lattice mismatches between the two ZnSe layers. Such type of interfacing increased the lattice parameters and decreased the stress (S) compared to single metal sandwiched films. However, it has no effect on the grain size (*D*), stacking fault (*SF*), dislocation density (δ) and micro-strain (ε). For YAu layers, the lattice mismatch between face centered cubic-Y and face centered cubic-Au is ~ found to be 20% along the *a*-axes. The lattice mismatch at the YAu interface is an additional condition in the structure of ZnSe.

The increase in the ZnSe lattice parameters which we observe for ZnSe/Au/ZnSe and ZnSe/YAu/ZnSe sandwiched films is also observed for Cobalt doped ZnSe [18] and Eu^{3+}- doped ZnSe [19]. It is reported that the increased Co- doping concentration increased the lattice parameters for ZnSe due to substitution of Co ion in Zn ion site [18]. The Eu^{3+} – doped ZnSe increased the lattice parameters from *a*= 3.915 Å and from *c*= 5.973 Å to *a*= 3.988 Å and *c*= 6.125 Å. This behavior was assigned to large ionic radii of Eu^{3+} (109 pm) which causes subsequent

deformation of ZnSe lattice [19]. The extension of the lattice constant is also reported for Al-doped ZnSe [20]. In our case, the extension in the lattice of ZnSe/Au/ZnSe and ZnSe/YAu/ZnSe may be attributed to the increase in the number of vacant sites in the ZnSe structure as a result of interstitial atomic substitutions which forces the lattice to expand and increases the lattice parameters. The data of Table 1 show that using of YAu double layers between ZnSe layers is preferable. It increased the lattice parameters and reduced the defects density more than the other sandwiched films.

The effects of the Y, Au and YAu nano-layers on the optical properties of ZnSe thin films is explored by means of ultraviolet-visible light spectroscopy. The measured transmittance and reflectance spectra are employed to identify the absorption coefficient (α) spectra through the previously reported equations [21]. The absorption coefficient as a function of incident photon energy for ZnSe, ZnSe/Y/ZnSe, ZnSe/Au/ZnSe and ZnSe/YAu/ZnSe are displayed in Fig. 2 (a). Three regions appeared in the spectra. These regions are the absorption saturation region above 3.00 eV, sharp region between 2.30 – 3.00 eV and transparent region below 2.3 eV. Pronounced effects of the nanosandwiching on the absorption coefficient (α) values are observed below 2.5 eV. In the region of 2.5-1.4 eV, α values for ZnSe are, approximately, the same as that of ZnSe/Y/ZnSe. Replacing Y by Au increases the values of α. The highest values of α are observed when double layers of YAu are used.
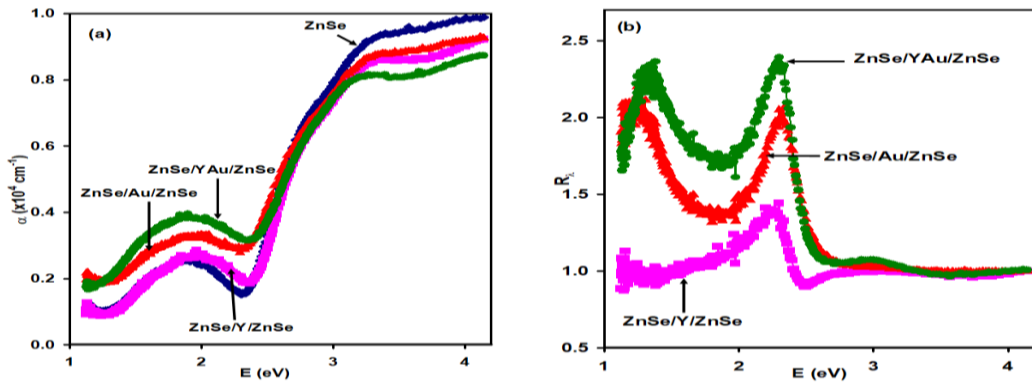

Fig. 2. (a) The absorption coefficients and (b) the absorbability (R_λ) spectra for ZnSe/Y/ZnSe, ZnSe/Au/ZnSe and ZnSe/YAu/ZnSe sandwiched films.

To obtain a more clear picture about the variations in the light absorbability of the films, the absorbability (R_λ) of the ZnSe/Y/ZnSe, ZnSe/Au/ZnSe and ZnSe/YAu/ZnSe nanosandwiched films are calculated from the ratio between the absorption coefficient values through the relation ($R_\lambda = \alpha_{ZnSe/x/ZnSe}/\alpha_{ZnSe}$), where x is Y, Au and YAu. The absorbability (R_λ) spectra are shown in Fig. 2 (b). As appears in the figure, the presence of Y layers between two ZnSe layers increases the light absorbability for Y sandwiched films by 1.4 times at 2.23 eV. This peak width is 0.53 eV. The absorbability was better when an Au layer was used to form ZnSe/Au/ZnSe sandwiched film. It exhibits maxima of 2.0 times at 2.32 eV. The width of the R_λ-E peak increased to 0.77 eV compared to that of ZnSe/Y/ZnSe. In addition, the ZnSe/Au/ZnSe light absorbability is also increased by 2.15 times at 1.24 eV. The existence of Y and Au stacked layers between two ZnSe layers enhanced the absorbability more than that of Y or Au alone. The ZnSe/YAu/ZnSe absorbability was increased by 2.4 times at 2.29 eV with peak width of 0.71 and by 2.3 times at 1.36 eV.

It is also noticeable from Fig. 2 (a) that, the absorption coefficient doesn't reach zero even in the transparent region. The nonzero values of α indicate the presence of the interbands or band tails. The band tails in the semiconductor are usually formed by impurities, inhomeganuities, defects and broken bonds. As the Fig. 2 (a) show, while the presence of the Y doesn't strongly affect the already existing interband of ZnSe, the replacement of Au alter them significantly

causing higher degree of absorption, the coating of the Y with Au through the sandwiching process enhances them more. In the low absorption region, where the band tails is believed to exist, the α values in that region can be presented by the relation, $\alpha = \alpha_o \exp(E/E_e)$ [22]. Where, α_o is a constant and E_e is the band tail energy (or Urbach energy). The energy band tail usually indicates the presence of defects in the structure and the optical transition between localized and extended state in the valence and conduction bands. The E_e can be estimated from the reciprocal of the linear slope of $\ln(\alpha) - E$ variations [22] which are illustrated in Fig. 3 (a). The calculated values of the band tail energy is illustrated in Table 1. These bands tails energy levels may also be related to the recombination mechanism as a result of antisiting defects [23]. While the ZnSe/Y/ZnSe exhibits narrower band width compared to that of un-sandwiched ZnSe, the ZnSe/Au/ZnSe and ZnSe/YAu/ZnSe has wider band tails. We believe that this effect resulted from the orbital overlapping and valence electron contributions. The Au with the electronic configuration $6s^1 4f^{14} 5d^{10}$ can exhibit denser orbital overlapping compared to Y whose electronic configuration is $5s^2 4d^1$. While the gold ion contributes five valence electrons to the valence band of ZnSe, the Y supplies the valence band of ZnSe by three electrons.
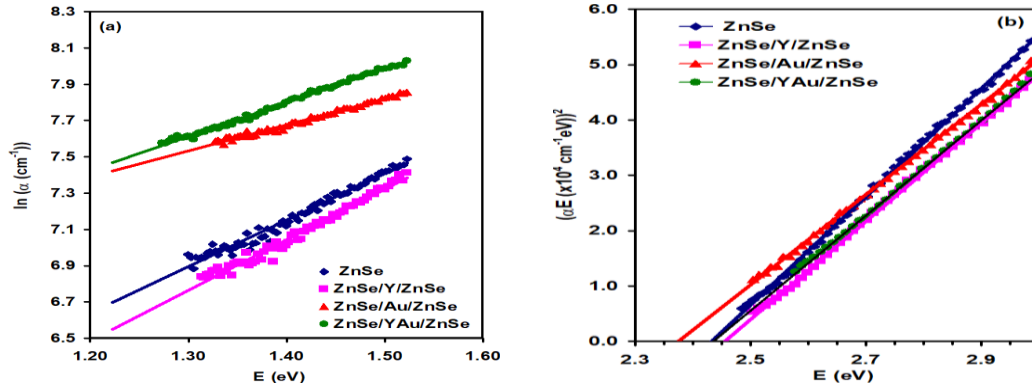

Fig. 3. (a) The $\ln(\alpha) - E$ variations and (b) The $(\alpha E)^2 - E$ for ZnSe,
ZnSe/Y/ZnSe, ZnSe/Au/ZnSe and ZnSe/YAu/ZnSe sandwiched films.

The absorption coefficient spectra reveal information about the energy gap (E_g) of ZnSe, ZnSe/Y/ZnSe, ZnSe/Au/ZnSe and ZnSe/YAu/ZnSe. The optical energy gap for the direct allowed electronic transitions is estimated from the absorption coefficient spectra by applying the well-known Tauc's relation $(\alpha E)^2 = A (E - E_g)$, where A is a constant and E_g is the energy band gap. The $(\alpha E)^2 - E$ variations reveal the energy band gap value that are shown in Table 1. The direct allowed energy band gap of the hexagonal ZnSe is 2.44 eV. The direct energy band gap for the ZnSe has a highest valance band at the Γ_{15} point which split because of the spin orbit coupling into a two-fold Γ_7 and a four-fold Γ_8 state. Thus, the band gap should be considered as the transition from Γ_{7v} or Γ_{8v} valence band state to Γ_{6c} conduction band state [23].

The literature data reported an energy band gap value in the region of 2.55-2.70 eV for direct allowed transition type of ZnSe [24, 25]. In addition, the allowed direct energy band gap of ZnSe increases to 2.46 eV via Y nanosandwiching and decreased to 2.38 eV when Au replaces Y. Moreover, it observed that the direct allowed E_g of ZnSe/YAu/ZnSe is 2.44 eV, which is similar to that of ZnSe. The slight attenuations in the energy band gap values are of less importance in this work and may be ascribed to the image force lowering at the Y, Au and YAu ZnSe interfaces. G. M. Lohar et al. reported an energy band gap value of 2.45 for Fe-doped ZnSe [8]. In addition an energy gap values in the range of 2.81-2.77 are reported for Eu-doped ZnSe [25]. These high values for Eu-doped ZnSe are due to the incorporation of Eu^{3+} ions onto the ZnSe structure or to the phonons interactions [25].

Table 1. The structural parameters of ZnSe, ZnSe/Y/ZnSe, ZnSe/Au/ZnSe and ZnSe/YAu/ZnSe sandwiched films.

	ZnSe	ZnSe/Y/ZnSe	ZnSe/Au/ZnSe	ZnSe/YAu/ZnSe
2θ (°)	28.1	28.1	28	27.8
I $(a.u.)$	727	844	922	1333
d (Å)	3.177	3.177	3.188	3.210
(hkl)	(002)	(002)	(002)	(002)
a (Å)	4.051	4.051	4.066	4.082
c (Å)	6.354	6.354	6.376	6.421
D (nm)	28.54	21.41	21.41	28.53
SF(%)	0.265	0.353	0.354	0.266
S $(\times 10^{10})(dy/cm^2)$	3.12	3.12	2.73	1.93
δ $(\times 10^{11})$ $(line/cm^2)$	4.33	7.69	7.69	4.33
$\varepsilon(\times 10^{-3})$	5.23	6.97	7.00	5.29
$E_e(eV)$	0.41	0.35	0.65	0.54
$E_g(eV)$	2.44	2.46	2.38	2.44

The band gap energy values have slightly changed by nanosandwiching. A band gap narrowing occurs. M. Harb et al. reported that the formations of incompletely delocalized electronic levels over valence band states are responsible for the band gap narrowing of S-doped TiO_3 [26]. In addition, the lattice distortion induced by the dopant atom was also assigned as a reason for the direct band gap narrowing [27]. These effects of the nanosandwiched materials on the energy band gap values can also be attributed to the structural modifications like decrease in the grain size, differences in the electron affinity values of ZnSe (3.8 eV) [20] and Y and Au metals, large lattice mismatch, defects, impurity level and incomplete bonds in the films structure.

To explain the patterns that had emerged in the reflection spectra and investigate the possible applications of the nanosandwiched films, the dielectric properties of ZnSe, ZnSe/Y/ZnSe, ZnSe/Au/ZnSe and ZnSe/YAu/ZnSe structures are also investigated. The effective dielectric constant ε_{eff} is determined through the relation [27]:

$$R = \frac{\left(\sqrt{\varepsilon_{eff}}-1\right)^2 + \left(\frac{\alpha\lambda}{4\pi}\right)^2}{\left(\sqrt{\varepsilon_{eff}}+1\right)^2 + \left(\frac{\alpha\lambda}{4\pi}\right)^2} \tag{1}$$

In this equation, R is the reflectance at normal incidence, ε_{eff} the effective dielectric constant, α and λ are the absorption coefficient and incident photon wavelength, respectively. The real (ε_r) and imaginary (ε_{im}) parts of dielectric constant can be determined from the data of the effective dielectric constant ε_{eff} through the formulas ($\varepsilon_r = \varepsilon_{eff} - (\frac{\alpha\lambda}{4\pi})^2$), and ($\varepsilon_{im} = \sqrt{\varepsilon_{eff}}(\frac{\alpha\lambda}{2\pi})$), respectively [27].

The real dielectric constant ε_r spectra for the studied samples are illustrated in Fig. 4. As the figure shows, the real part ε_r of the dielectric constant for ZnSe increases sharply with increasing photon energy reaching a maximum of ~10 at resonance frequency of 1.75 eV (inset of Fig. 4). This peak should correspond to the interband transition in ZnSe which arises from the inhomogeneity, defect and broken bonds on the structure as we discussed in the preceding part of this article. It could also be assigned to the direct allowed transitions in selenium which takes place at 1.75 eV [28]. The ε_r for ZnSe also exhibited two others resonating peaks with ε_r values of 8.56 and 6.12 corresponding to an energy value of 2.59 eV and 3.45 eV, respectively. The resonant peak of energy 2.59 eV can be attributed to direct allowed electronic transitions in ZnSe as it is close to the energy band gap values. On the other hand, the peak detected at 3.45 eV is

probably due to the interaction between oxygen atoms and zinc atoms. The Zn-O band is reported to exhibit direct electron transitions band gap of 3.40 eV [29]. The oxygen is present in the glass substrate which could cause Zn-O bonds at the ZnSe-glass interface.
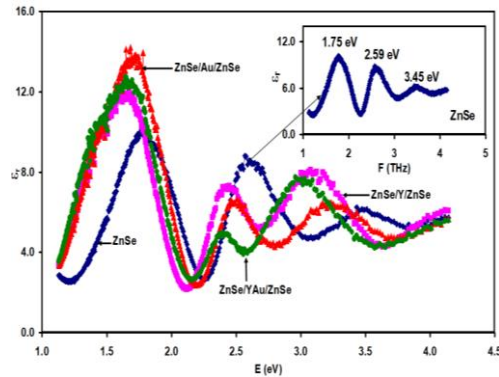

Fig. 4. The dielectric spectra for ZnSe, ZnSe/Y/ZnSe, ZnSe/Au/ZnSe and
ZnSe/YAu/ZnSe sandwiched films.

As it is also readable from Fig. 4, the nanosandwiching of the Y, Au and YAu between two layers of ZnSe improved the dielectric property of ZnSe. Particularly, for these nanosandwiched layers, the real part ε_r exhibits a maximum value of ~12, 13.82 and 12.57 at critical energy values of 1.68, 1.75 and 1.71 eV for the Y, Au and YAu sandwiched films, respectively. The other two peaks also shifts to 2.40, 2.46 and 2.37 eV and to 3.08, 3.20 and 2.99 eV, respectively. These improvements in the dielectric constant and shift in the critical energy values is preferable because it indicates more sensitivity to the light spectrum in the visible regions [27]. While the presence of Y increased the maximum value of ε_r from ~10 to ~12, and the Au increased it from ~10 to ~14. The YAu appeared less effective, it increased the ε_r from ~10 to ~13. The decreasing value of ε_r with the presence of YAu is probably due to less contribution of charge accumulation at the interface of the films compared to ZnSe/Au/ZnSe which is more effective.

The imaginary part ε_{im} of dielectric constant spectra gives significant information about the optical conductivity, electronic motion and the electron-Plasmon interaction in ZnSe sandwiched films. The ε_{im} for the ZnSe, ZnSe/Y/ZnSe, ZnSe/Au/ZnSe and ZnSe/YAu/ZnSe nanosandwiched films are illustrated in Fig. 5. It is clear from the figure that the ε_{im} exhibits two orders of magnitude lower than those of real part. The ε_{im} spectra of ZnSe exhibited three resonating peaks at 1.77 eV, 2.72 eV and at 3.41 eV. For ZnSe/Y/ZnSe, the imaginary part shifted to lower resonance energy. Also, the peak which appeared at 2.72 eV for ZnSe disappeared in ZnSe/Y/ZnSe sandwiched film. While the resonant peaks of ε_{im} for ZnSe/Y/ZnSe are formed at 1.69 eV and 3.10 eV, those of ZnSe/Au/ZnSe exhibits larger values and are formed at 1.70 eV, 2.57 eV and 3.20 eV. The ε_{im} for ZnSe/YAu/ZnSe exhibited similar trend of variation but with higher values. The maximum ε_{im} value for ZnSe/YAu/ZnSe is 0.15 at 1.64 eV. The second resonating peak for this structure exists at 3.01 eV.
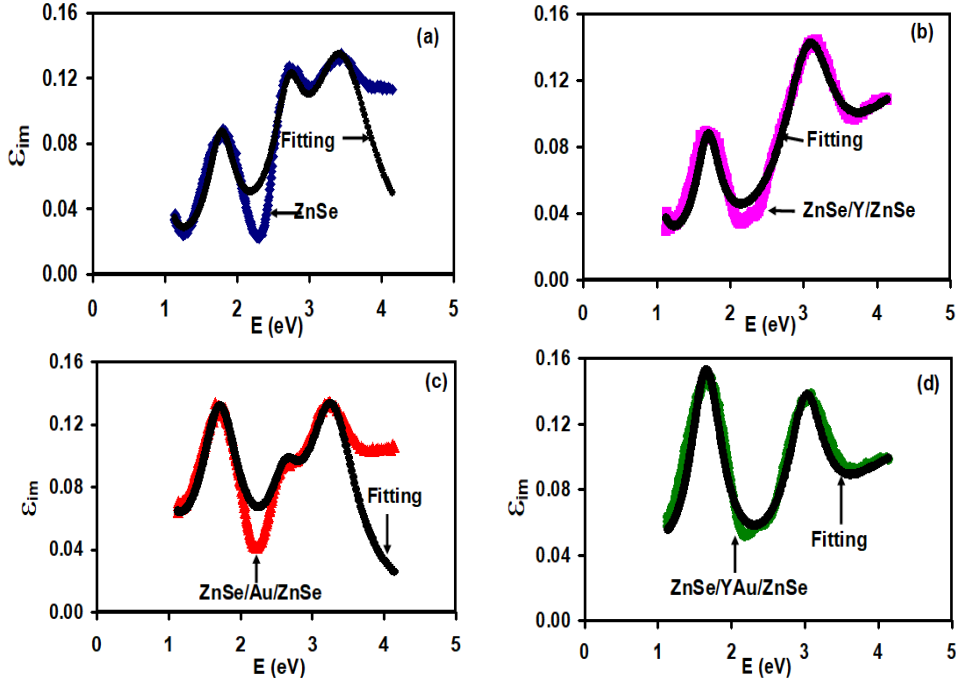
Fig. 5. The imaginary part of the dielectric spectra for (a) ZnSe, (b) ZnSe/Y/ZnSe, (c) ZnSe/Au/ZnSe and (d) ZnSe/YAu/ZnSe nanosandwiched films. The black colored plots represent the fitting which is achieved by Eqn. (2).

In order to understand the reason for the resonance peaks which appeared in the imaginary part of the dielectric spectra, and explore information about the Plasmon-electron interactions in these structures, the ε_{im} spectra are reproduced in accordance with Drude-Lorentz approach for optical conduction through the relation [30],

$$\varepsilon_{im}(\omega) = \sum_{i=1}^{K} \frac{\omega_{pe_i}^2 \omega}{\tau((\omega_{ei}^2 - \omega^2)^2 + \omega_i^2 \tau_i^{-2})} \tag{2}$$

Here, τ is being the electron scattering time, ω is the angular frequency, ω_e reduced resonant frequency and $\omega_{pe} = \sqrt{4\pi n e^2/m^*}$ is the electron bounded plasma frequenc, n is the free electron density and m^* is the effective mass of electron. In addition, the frequency independent drift mobility, which results from the incident electromagnetic field interaction with the films, can be determined by the formula $\mu = e\tau/m^*$. Eqn. (2) provide information about the values of the $\tau, \omega_e, \omega_{pe}, n, and \mu$ for the studied samples. The electron bounded plasma frequency which is resonant oscillation of conduction electrons at the interface between two ZnSe layers and Y or Au metal, or between the two metals (YAu) can be excited by incident light waves. The resonance in the dielectric spectra donated when the frequency of incident light wave equals the free surface charge carrier natural frequency ω_e. The surface free charge carriers which oscillate against the restoring force of positive nuclei cease when the energy is lost in the electronic friction that leads to a damping force of coefficient $\gamma = \tau^{-1}$ [21, 27].

In Eqn. (2), K is the number possible linear oscillators. The experimental data was fitted by substituting the effective mass values as $m^*_{ZnSe} = 0.16m_o$ [23], $m^*_Y = 1.05m_o$ [31], and $m^*_{Au} = 1.10m_o$ [31]. The effective mass of ZnSe film was evaluated from the equation $m^*_{ZnSe/ZnSe} = (2/m^*_{ZnSe})^{-1} = 0.080m_o$. For the three layers ZnSe/Y/ZnSe, it was found to be $m^*_{ZnSe/Y/ZnSe} = (2/m^*_{ZnSe} + 1/m^*_Y)^{-1} = 0.074m_o$. Thus, the effective mass of ZnSe/Au/ZnSe and ZnSe/YAu/ZnSe were also calculated as $0.075m_o$ and $0.069m_o$, respectively. The theoretical data of ε_{im} spectra donated by the black colored fitting curve are shown in Fig. 5 for ZnSe, ZnSe/Y/ZnSe, ZnSe/Au/ZnSe and ZnSe/YAu/ZnSe sandwiched films. The black solid

lines in Fig. 5 indicate a good agreement between the experimental and theoretical data values of imaginary dielectric constant. The fitting parameters which produce the theoretical imaginary part in accordance with Eqn. (2) are tabulated in Table 2.

Table 2. The optical conduction parameters for electron-Plasmon interactions at the ZnSe, ZnSe/Y/ZnSe, ZnSe/Au/ZnSe and ZnSe/YAu/ZnSe sandwiched films.

	ZnSe				ZnSe/Y/ZnSe				ZnSe/Au/ZnSe				ZnSe/YAu/ZnSe			
m^*/m_o	0.0801				0.0744				0.0746				0.0697			
$\tau_i(fs)$	5.00	1.40	1.30	0.60	4.00	1.60	0.80	0.29	1.00	1.00	1.20	0.80	7.00	1.20	1.10	0.25
n (x 10^{17} cm^{-3})	2.00	2.70	4.60	22.0	1.50	2.00	11.0	46.0	2.50	5.50	3.00	14.0	9.00	4.80	6.50	46.0
ω_{ei}(x$10^{15}Hz$)	1.30	2.72	4.13	5.28	1.30	2.60	4.70	7.00	1.00	2.65	4.00	5.00	0.60	2.55	4.60	7.00
ω_{pei} (GHz)	0.94	1.09	1.42	3.11	0.84	0.97	2.28	4.67	1.09	1.61	1.19	2.57	2.13	1.56	1.81	4.83
$\mu(cm^2/Vs)$	1098	308	285	132	945	378	189	69	236	236	283	189	1766	303	227	63
$\sigma(\Omega cm)^{-1}$	35.1	13.3	21.0	46.4	22.7	12.1	33.3	50.4	9.43	20.7	13.6	42.2	254.0	23.2	28.9	46.4

The electron scattering time for ZnSe decreased when Y or Au layer existed between two ZnSe layers from 5.0 fs to 4.0 fs and to 1.0 fs, respectively. The drift mobility which exhibit value of 1098 cm^2/Vs for ZnSe decreased to 945 cm^2/Vs and to 236 cm^2/Vs upon nanosandwiching of ZnSe with Y and Au, respectively. The electron scattering time and drift mobility for ZnSe/YAu/ZnSe increased to 7.0 fs and to 1766 cm^2/Vs , respectively. This enhancement in the drift mobility of ZnSe is assigned to the high scattering time, and to the carrier concentration variation that is associated with the amount of defects [32]. The two metals layer with different vacancies reduced the amount of defect which facilitated the movement of freer electrons. In scope of these observations, the improvement of μ for ZnSe/YAu/ZnSe may be due to reduced dislocation density as seen from XRD analysis. The resulting values agree with literature data of ZnSe, which shows that the mobility can be up to 400 cm^2/Vs [23].

In addition, the free electron density for ZnSe, ZnSe/Y/ZnSe, ZnSe/Au/ZnSe and ZnSe/YAu/ZnSe are found to be 2.00 x 10^{17} cm^{-3}, 1.20 x 10^{17} cm^{-3}, 2.50 x 10^{17} cm^{-3} and 9.0 x 10^{17} cm^{-3}, respectively. The free electron density values suggest the consistency between the structural results and the dielectric analysis. Particularly, the decrease in the stress value upon YAu sandwiching is associated with freer electrons. Both result support the belief that the use of stacked layers improves the optical and dielectric performance of ZnSe. Moreover, the electron bounded plasma frequency ω_{pe} and the reduced resonance frequency ω_e increases for ZnSe/YAu/ZnSe sandwiched films and decreases for ZnSe/Y/ZnSe and ZnSe/Au/ZnSe. G. I. Rusu et al. reported that the ZnSe has a donor concentration (N_D) of 3.67×10^{17} cm^{-3} which is consistent with the dielectric data that are shown in Table 4.3 [33].

As shown in Table-2, it is clear that YAu sandwiching improves the optical conduction parameters more than those of Y and Au sandwiching alone. This high value of the ZnSe/YAu/ZnSe mobility corresponds to the large scattering time values of 7.0 fs, and so, less damping rate and less resistance. The high mobility of ZnSe/YAu/ZnSe makes it a better candidate as a thin film transistor. The free electron density n, reduced resonant frequency ω_e and the bounded Plasmon frequency ω_{pe} increased when the YAu sandwiching is used. This increase corresponds to the presence of further free electrons on the metal surface [27]. In addition, the values of the electron bounded Plasmon frequency ω_{pe} for ZnSe, ZnSe/Y/ZnSe, ZnSe/Au/ZnSe and ZnSe/YAu/ZnSe films are improved in the range of $0.94 - 4.83$ GHz. The reduced resonance frequency ω_e is also increased from 1.30 x$10^{15}Hz$ to 7.00 x$10^{15}Hz$. The interference of Plasmon frequency with the films reveals more information about the ac-signal or electromagnetic wave. For a gigahertz plasma frequency level, the microwave propagating through these films can be transmitted only if they have frequencies higher than ω_{pe}. Since the computed ω_{pe} values are in the range of $0.94 - 4.83$ GHz, the ZnSe, ZnSe/Y/ZnSe, ZnSe/Au/ZnSe and ZnSe/YAu/ZnSe

films can be employed as wave traps of at least four resonant frequencies which suits microwave communications [21, 27].

It is also worth of consideration that the Ag nanosandwiched ZnSe thin films [6] which are prepared by the electron beam evaporation technique exhibited much lower mobility values compared to those we obtained by Y, Au and YAu nanosandwiching. The density of free carriers for the ZnSe/Ag/ZnSe is reported to be $1.2 \times 10^{20}\ cm^{-3}$. This value is higher than those we obtained in this study. Our values are more appropriate for device fabrication. In addition, the indium nanosandwiching between two layers of ZnSe which show good microwave filtering properties [11] is also reported to exhibit enhanced the light absorbability at 2.38 eV by 13.8 times [7]. This value is higher than that we obtained in this study. However, as there is no information about the dielectric performance of the ZnSe/In/ZnSe thin films, the optical conductivity parameters reported in this work represent novelty of the Y, Au and YAu sandwiched films over other sandwiching or doping studies on ZnSe.

4. Conclusions

In this work, we attempted to alter the structural, optical and dielectric properties of ZnSe thin films via the nanosandwiching technique. The gold, yttrium and yttrium-gold metal slabs are selected for this purpose. The presence of these metals as sandwiched layers in the structure of ZnSe displayed positive effect on the light absorbability and increased the interbands in the films. In addition, while the presence of single metal layer decreased the drift mobility, using two different stacked metallic layers (YAu) significantly increased the drift mobility and reduced the electronic friction in the films. As an additional enhancement in the performance of the ZnSe thin films, the presence of Y, Au and YAu in the films extends the plasmon frequency range and make it reach 4.83 GHz. This property makes the metal nanosandwiched ZnSe more appropriates for use as dual device which exhibit responsivity to visible light and also behave as microwave cavities.

References

[1] H. H. Kurt, Journal of Electronic Materials **47**(8), 1 (2018).
[2] S. V. Averin, P. I. Kuznetzov, V. A. Zhitov, L. Y. Zakharov, V. M. Kotov, Optical and Quantum Electronics **50**(10), 368 (2018).
[3] Y. L. Sun, D. Xie, M. X. Sun, C. J. Teng, L. Qian, R. S. Chen, L. Xiang, T. L. Ren, Scientific reports **8**(1), 5107 (2018).
[4] S. Dai, G. Feng, H. Zhang, S. Ning, Y. Xiao, S. Zhou, Optics letters **43**(3), 411 (2018).
[5] R. Zhou, S. Sun, C. Li, L. Wu, X. Hou, P. Wu, ACS Applied Materials & Interfaces **10**(40), 34060 (2018).
[6] X. Y. Song, W. T. Zhang, F. Li, Y. L. Liu, Acta Photonica Sinica **40**(6), 857 (2011).
[7] S. E. Al Garni, A. F. Qasrawi, Results in physics **7**, 4168 (2017).
[8] G. M. Lohar, S. T. Jadhav, H. D. Dhaygude, M. V. Takale, R. A. Patil, Y. R. Ma, M. C. Rath, V. J. Fulari, Journal of Alloys and Compounds **653**, 22 (2015).
[9] C. Bothe, A. Kornowski, H. Tornatzky, C. Schmidtke, H. Lange, J. Maultzsch, H. Weller, Journal of the German Chemical Society **54**(47), 14183 (2015).
[10] N. Priyadharsini, M. Elango, S. Vairam, T, Venkatachalam, M. Thamilselvan, Optik-International Journal for Light and Electron Optics **127**(19), 7543 (2016).
[11] S. E. Al Garni, Chalcogenide Letters **14**(12), 545 (2017).

[12] M. Maczka, P. Pasierb, Materials Research Bulletin **87**, 84 (2017).

[13] Q. Yuan, J. Wu, C. Qin, A. Xu, Z. Zhang, Y. Lin, Z. Chen, S. Lin, Z. Yuan, X. Ren, P. Zhang, Materials Chemistry and Physics **199**, 122 (2017).

[14] A. P. Hagen, Inorganic Reactions and Methods, John Wiley & Sons USA (2009).

[15] J. Dakin, R. G. Brown, Handbook of Optoelectronics, CRC Press USA (2006).

[16] D. Sahu, N. R. Panda, B. S. Acharya, A. K. Panda, Optical Materials **36**(8), 1402 (2014).

[17] Harald Ibach, Hans Luth, Solid state physics: An Introduction to principles and material science, Springer-Velag Berlin Heideberg (2009).

[18] P. Mallikarjuna, J. Sivasankar, M. R. Begam, N. M. Rao, S. Kaleemulla, J. Subrahmanyam, Materials Science and Engineering **9**, 2412 (2017).

[19] T. R. Kumar, P. Prabukanthan, G. Harichandran, J. Theerthagiri, S. Chandrasekaran, J. Madhavan, Ionics **23**(9), 2497 (2017).

[20] P. Prathap, N. Revathi, Y. V. Subbaiah, K. R. Reddy, R. W. Miles, Solid State Sciences **11**(1), 224 (2009).

[21] S. R. Alharbi, A. F. Qasrawi, Current Applied Physics **17**(6), 835 (2017).

[22] G. A. Evingur, O. Pekcan, Composite Structures **183**, 212 (2018).

[23] O. Madelung, Semiconductor: Data Handbook, Springer NewYork (2004).

[24] E. R. Shaaban, I. S. Yahia, E. R. Sharaf, Journal of Electronic Materials **46**(1), 527 (2017).

[25] M. M. Ivashchenko, A. S. Opanasyuk, I. P. Buryk, V. A. Lutsenko, A. V. Shevchenko, Journal of Nano-and Electronic Physics **9**(1), 1011 (2017).

[26] M. Harb, P. Sautet, P. Raybaud, Journal of Physical Chemistry C **117**(17), 8892 (2013).

[27] O. A. Omareya, A. F. Qasrawi, S. E. Al Garni, Physica B **520**, 57 (2017).

[28] S. N. F. M. Nasir, H. Ullah, M. Ebadi, A. A. Tahir, J. S. Sagu, M. A. Mat Teridi, Journal of Physical Chemistry C **121**(11), 6218 (2017).

[29] W. A. Hadi, M. S. Shur, S. K. O'Leary, Journal of Materials Science: Materials in Electronics **25**(11), 4675 (2014).

[30] M. Eldlio, F. Che, M. Cada, IAENG Transactions on Engineering Technologies: Springer **247**, 41 (2014).

[31] S. R. Alharbi, A. F. Qasrawi, Optik **136**, 524 (2017).

[32] T. Y. Abed, A. F. Qasrawi, S. E. Al Garni, Journal of Alloys and Compounds **731**, 1022 (2018).

[33] G. I. Rusu, M. E. Popa, G. G. Rusu, I. Salaoru, Applied Surface Science **218**(1-4), 223 (2003).